Computers in Biology and Medicine 129 (2021) 104135

Contents lists available at ScienceDirect

Computers in Biology and Medicine

journal homepage: http://www.elsevier.com/locate/compbiomed

Radiomics-based machine learning model to predict risk of death within 5-years in clear cell renal cell carcinoma patients

Mostafa Nazari [a], Isaac Shiri [b], Habib Zaidi [b,c,d,e,*]

[a] Department of Biomedical Engineering and Medical Physics, Shahid Beheshti University of Medical Sciences, Tehran, Iran
[b] Division of Nuclear Medicine and Molecular Imaging, Geneva University Hospital, CH-1211, Geneva 4, Switzerland
[c] Geneva University Neurocenter, Geneva University, Geneva, Switzerland
[d] Department of Nuclear Medicine and Molecular Imaging, University of Groningen, University Medical Center Groningen, Groningen, Netherlands
[e] Department of Nuclear Medicine, University of Southern Denmark, Odense, Denmark

ARTICLE INFO

Keywords:
Radiomics
Machine learning
CT
Survival prediction
Renal cell carcinoma

ABSTRACT

Purpose: The aim of this study was to develop radiomics–based machine learning models based on extracted radiomic features and clinical information to predict the risk of death within 5 years for prognosis of clear cell renal cell carcinoma (ccRCC) patients.

Methods: According to image quality and clinical data availability, we eventually selected 70 ccRCC patients that underwent CT scans. Manual volume-of-interest (VOI) segmentation of each image was performed by an experienced radiologist using the 3D slicer software package. Prior to feature extraction, image pre-processing was performed on CT images to extract different image features, including wavelet, Laplacian of Gaussian, and resampling of the intensity values to 32, 64 and 128 bin levels. Overall, 2544 3D radiomics features were extracted from each VOI for each patient. Minimum Redundancy Maximum Relevance (MRMR) algorithm was used as feature selector. Four classification algorithms were used, including Generalized Linear Model (GLM), Support Vector Machine (SVM), K-nearest Neighbor (KNN) and XGBoost. We used the Bootstrap resampling method to create validation sets. Area under the receiver operating characteristic (ROC) curve (AUROC), accuracy, sensitivity, and specificity were used to assess the performance of the classification models.

Results: The best single performance among 8 different models was achieved by the XGBoost model using a combination of radiomic features and clinical information (AUROC, accuracy, sensitivity, and specificity with 95% confidence interval were 0.95–0.98, 0.93–0.98, 0.93–0.96 and ~1.0, respectively).

Conclusions: We developed a robust radiomics-based classifier that is capable of accurately predicting overall survival of RCC patients for prognosis of ccRCC patients. This signature may help identifying high-risk patients who require additional treatment and follow up regimens.

1. Introduction

Renal cell carcinoma (RCC) is the most commonly occurring type of kidney cancer and accounts for approximately 2% of all cancer deaths worldwide [1]. The 5-year survival rate for localized tumor is 93% and declines to 69% and 12% if it spreads to the lymph nodes and distant parts of body, respectively [2]. Among the different histologic subtypes, patients with clear cell RCC (ccRCC) proved to have a worse prognosis than other histological subtypes (pRCC and crRCC) [3,4].

Prognostication modeling could potentially be exploited for determining new and appropriate treatments for personalized medicine [5]. For this purpose, several prognostic models were investigated for RCC tumors [6]. The TNM staging system was designed to provide prognostic information [7,8]. To improve the predictive power of this system, the International Union Against Cancer (UICC) proposed a new prognostic model based on the TNM system that has gone through several modifications [9–12]. Another model introduced specifically for ccRCC tumors is the Stage, Size, Grade, and Necrosis (SSIGN) Score [13]. Nevertheless, their use in clinical practice is not completely satisfactory [14]. In addition, gene expression profiling to identify biomarkers for prognosis prediction is another active and appealing research area [15,16]. However, due to intra-tumor heterogeneity, invasive biopsy-based genomic analysis has poor prognostic prediction ability [17].

Radiomics is a multi-step process enabling to convert medical images

* Corresponding author. Geneva University Hospital, Division of Nuclear Medicine and Molecular Imaging, CH-1211, Geneva, Switzerland.
E-mail address: habib.zaidi@hcuge.ch (H. Zaidi).

https://doi.org/10.1016/j.compbiomed.2020.104135
Received 2 August 2020; Received in revised form 21 October 2020; Accepted 11 November 2020
Available online 23 November 2020

into high-dimensional and mineable structures, thus allowing a comprehensive analysis of whole regions of interest and correlation with clinical, diagnostic and prognostic information [18–20]. Standardized radiomics analysis includes image acquisition, reconstruction, image preprocessing, image processing, followed by feature extraction, selection, and classification/regression modeling [21,22]. In conventional radiomics studies, image preprocessing, processing and feature extraction steps can be performed using conventional image processing and handcrafted features extraction followed by established machine learning algorithms. However, in deep learning studies, these steps can be automatically performed using convolutional deep neural networks (CNNs) [22–27].

Radiomics analysis is widely employed in oncology [28,29], neurology [30–34], and cardiovascular diseases [35–39] using different imaging modalities, including CT, MRI, SPECT and PET [40]. Radiomics-based prognostic models have proved useful to predict patient prognosis for interventional procedures and therapies and for monitoring response to treatment in many cancer types, including hepatocellular carcinoma [41], pituitary macroadenoma [42], prostate cancer [43], non-small cell lung cancer [44–47], head and neck cancer [48,49], breast cancer [28], and glioma [29,50,51].

Haider et al. [52] analyzed CT texture-based quantitative imaging biomarkers for survival prediction in patients with metastatic clear cell carcinoma using a Cox regression model to assay correlation of texture parameters with measured time to progression and overall survival. The results indicated that normalized standard deviation (SD) and entropy is correlated with survival. Lubner et al. [53] developed a model for correlating CT texture features with oncologic outcomes and reported that the SD, mean positive pixels, and entropy texture are significantly associated with ccRCC tumor prognosis. Tabibu et al. [54] developed a framework for survival prediction using digital histopathological images and deep learning algorithms for RCC patients. The results demonstrated that risk indexing using Lasso regularized Cox algorithm based on tumor shape and nuclei features provided an accurate prognostic model. The main aim of the current work was to develop radiomics-based machine learning models using the extracted features and clinical information to predict the risk of death within 5-years for prognosis of ccRCC patients.

2. Materials and methods

The flowchart of the current study protocol is shown in Fig. 1.

2.1. Clinical studies

Two hundred and twenty-two CT iamges of patients from the cancer image archive (TCIA) database [55] were enrolled in this study protocol. According to image quality and clinical data availability, we eventually selected 70 ccRCC patients that underwent CT scans. The clinicopathological characteristics of the patients are listed in Table 1.

2.2. Image acquisition

All patients underwent a three-phase helical CT scan routinely used to image the kidneys consisting of an unenhanced phase (pre-contrast), a corticomedullary phase (40–70 s delay) and a nephrographic phase (100–120 s delay) after intravenous injection of 100–150 ml of iso-osmolar contrast material. For all patients, CT scans were performed with 120 kVp tube potential and 150–300 mAs tube current. Image reconstruction was performed using a filtered backprojection algorithm.

2.3. Tumor segmentation

Manual volume-of-interest (VOI) segmentation of all images was performed using the 3D slicer software package [56] and verified by an experienced radiologist. We carefully delineated optimal-sized VOIs to avoid partial volume effect on features calculation.

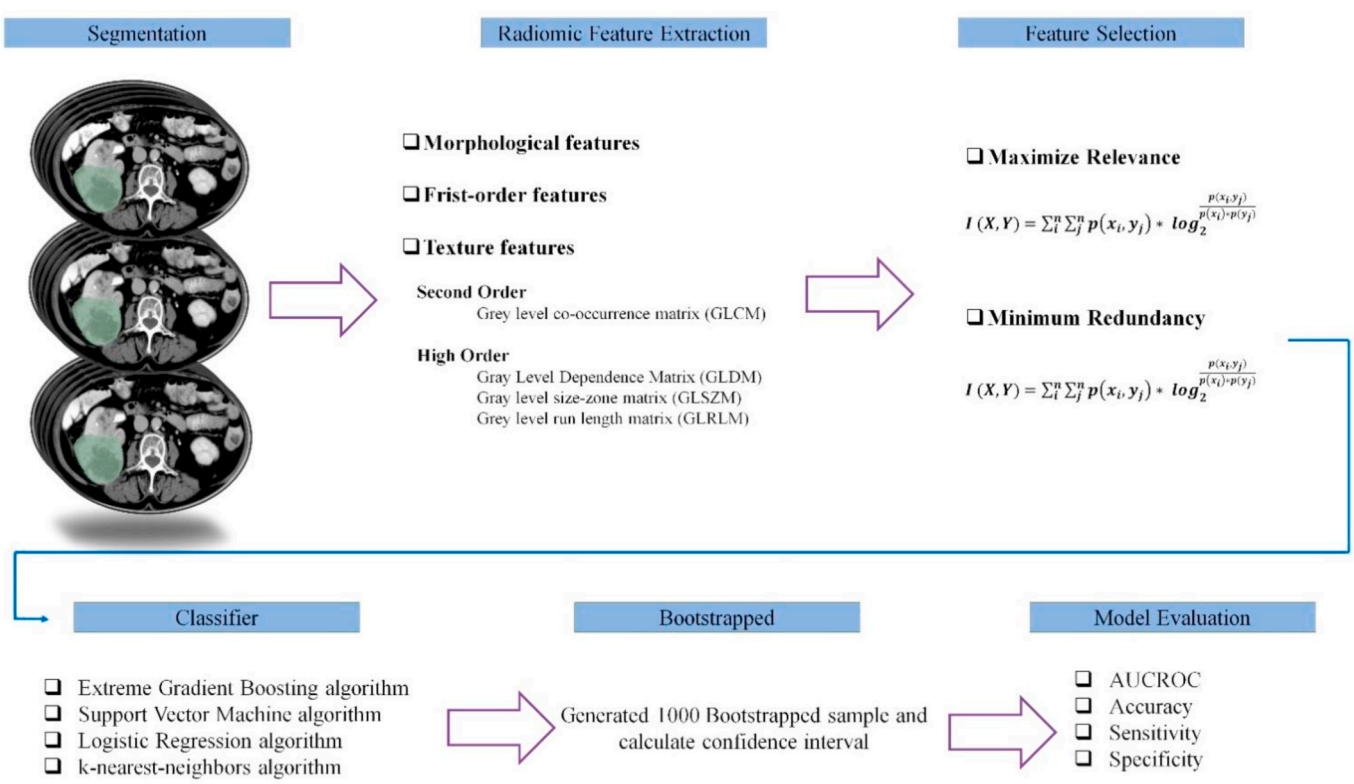

Fig. 1. Flowchart of the current study protocol.

Table 1
Patients' clinicopathological characteristics.

Characteristic	Number (%)
Patients' status in 5-years follow up	
Alive	51 (73%)
Dead	19 (27%)
Patient's stage	
Stage I	41 (59%)
Stage II	7 (10%)
Stage III	16 (23%)
Stage IV	6 (8%)
Patient's grade	
G1	0
G2	30 (43%)
G3	33 (47%)
G4	7 (10%)
Sex	
Male	19 (27%)
Female	51 (73%)
Average age	60.5

2.4. Image pre-processing and feature extraction

We extracted radiomic features using the PyRadiomics open source python library [57]. Prior to feature extraction, all images were pre-processed with the *Resize* method to resample the images into an isotropic dataset to allow comparison between image data from different samples and scanners [58]. Image pre-processing was performed on images to extract different image features, including wavelets (with all possible combinations of High and Low pass frequency, with decompositions of HHH, HHL, HLH, HLL, LHH, LHL, LLH), Laplacian of Gaussian (LoG) using different sigma values to extract fine, medium, and coarse features, 0.5 to 5 with a step of 0.5), and resampling of the intensity values to 32, 64 and 128 bin levels [59]. All image pre-processing was performed on the segmented volume.

Overall, 2544 3D radiomics features were extracted from each VOI of each patient. The extracted features were categorized into shape and size (morphological feature), intensity histogram (first-order), second-order texture, including gray-level co-occurrence matrix (GLCM), and high-order texture features, including gray-level run-length matrix (GLRLM), gray-level size-zone matrix (GLSZM) and gray-level dependence matrix (GLDM).

2.5. Features selection

In radiomics, a large number of quantitative features are typically extracted from regions-of-interest. However, not all features are discriminative and many are highly correlated with each other, or even irrelevant, which might reduce the model's performance and maximize the computational cost. Selecting a subset of optimal features from the all extracted features is a critical step in radiomics model construction. In this study, we used the Minimum Redundancy Maximum Relevance (MRMR) algorithm. The idea of minimum redundancy is to select the features that have a minimal dependency with each other and maximum relevance as indicated by high mutual information with dependent variables. The motivation behind the choice of this method is its popularity in the literature, computational efficiency, and potential usage by the medical imaging community (publicly available open source software).

2.6. Classification

We classified the patients into high- and low-risk groups based on 5-years follow-up [60]. The patients who died within 5-years were assigned to the high-risk group whereas those who were alive further 5-years were classified in the low-risk group. In our study, four classification algorithms were used, including the Generalized Linear Model (GLM), Support Vector Machine (SVM), K-nearest Neighbor (KNN) and XGBoost algorithms. Tuning the hyperparameters of every classifier through an iterative grid search procedure to maximize the model's performance. The Leave-one-out cross-validation (LOOCV) resampling technique was applied in order to tune the model parameters.

2.7. Model validation

Owing to the limited dataset size, we used the Bootstrap resampling method (iterative resampling with replacement) to create validation sets. In our work, the area under the receiver operating characteristic (ROC) curve (AUROC), accuracy, sensitivity, and specificity were used to assess the performance of the classification models. Feature selection, model building and evaluation were performed using the R programming language (version 3.5.2).

Table 2
Area under the receiver operating characteristic (ROC) curve (AUROC), Accuracy, Sensitivity and Specificity with 95% CI for radiomics and Radiomics + Clinic for different image feature sets using the SVM model.

SVM	AUROC (95% CI)		Accuracy (95% CI)		Sensitivity (95% CI)		Specificity (95% CI)	
Image	Radiomics	Radiomics + Clinic	Radiomics	Radiomics + Clinic	Radiomics	Radiomics + Clinic	Radiomics	Radiomics + Clinic
Original image	0.68–0.73	0.80–0.83	0.75–0.78	0.77–0.79	0.19–0.23	0.18–0.23	0.97–0.98	~1
32_bin	0.79–0.82	0.85–0.88	0.77–0.79	0.83–0.85	0.18–0.23	0.44–0.50	~1	0.97–0.98
64_bin	0.75–0.79	0.83–0.86	0.72–0.74	0.79–0.81	~0	0.29–0.34	~1	0.97–0.98
128_bin	0.71–0.74	0.82–0.85	0.71–0.74	0.71–0.74	~0	~0	~1	~1
LoG_sigma.0.5	0.77–0.80	0.89–0.91	0.74–0.77	0.84–0.86	0.08–0.11	0.50–0.55	~1	0.97–0.98
LoG_sigma.1.0	0.66–0.71	0.83–0.86	0.71–0.73	0.81–0.83	~0	0.38–0.44	~1	0.97–0.98
LoG _sigma.1.5	0.73–0.77	0.88–0.9	0.80–0.82	0.80–0.82	0.34–0.39	0.35–0.40	0.97–0.98	0.97–0.98
LoG _sigma.2.0	0.70–0.73	0.86–0.88	0.75–0.78	0.71–0.74	0.13–0.17	~0	~1	~1
LoG _sigma.2.5	0.66–0.70	0.82–0.85	0.74–0.76	0.80–0.82	0.13–0.17	0.34–0.39	0.97–0.98	0.97–0.98
LoG _sigma.3.0	0.65–0.69	0.75–0.78	0.71–0.73	0.77–0.79	~0	0.23–0.28	~1	0.97–0.98
LoG _sigma.3.5	0.60–0.65	0.80–0.83	0.71–0.74	0.80–0.82	~0	0.33–0.39	~1	0.97–0.98
LoG _sigma.4.0	0.72–0.75	0.89–0.90	0.71–0.73	0.80–0.82	~0	0.34–0.39	~1	0.97–0.98
LoG _sigma.4.5	0.82–0.84	0.84–0.87	0.75–0.78	0.80–0.82	0.18–0.22	0.39–0.45	0.97–0.98	0.97–0.98
LoG _sigma.5.0	0.82–0.84	0.80–0.83	0.75–0.78	0.71–0.74	0.13–0.17	~0	~1	~1
Wav_HHH	0.76–0.79	0.77–0.81	0.71–0.73	0.83–0.85	~0	0.44–0.50	~1	0.97–0.98
Wav_HHL	0.71–0.75	0.86–0.89	0.71–0.74	0.83–0.85	~0	0.49–0.55	~1	0.95–0.96
Wav_HLH	0.75–0.78	0.81–0.85	0.77–0.79	0.81–0.83	0.23–0.28	0.39–0.44	0.97–0.98	0.97–0.98
Wav_HLL	0.72–0.76	0.86–0.89	0.76–0.78	0.80–0.82	0.29–0.34	0.38–0.44	0.93–0.95	0.95–0.96
Wav_LHH	0.77–0.80	0.87–0.89	0.71–0.74	0.72–0.75	~0	0.03–0.06	~1	~1
Wav_LHL	0.77–0.80	0.87–0.89	0.71–0.74	0.77–0.79	~0	0.18–0.23	~1	~1
Wav_LLH	0.77–0.80	0.88–0.90	0.71–0.74	0.85–0.86	~0	0.50–0.55	~1	0.97–0.98
Wav_LLL	0.71–0.75	0.78–0.81	0.71–0.74	0.72–0.75	~0	0.04–0.06	~1	~1

Table 3
Area under the receiver operating characteristic (ROC) curve (AUROC), Accuracy, Sensitivity and Specificity with 95% CI for radiomics and Radiomics + Clinic for different image feature sets using the KNN model.

KNN	AUROC (95% CI)		Accuracy (95% CI)		Sensitivity (95% CI)		Specificity (95% CI)	
Image	Radiomics	Radiomics + Clinic	Radiomics	Radiomics + Clinic	Radiomics	Radiomics + Clinic	Radiomics	Radiomics + Clinic
Original image	0.68–0.75	0.74–0.78	0.74–0.76	0.74–0.77	0.33–0.39	0.13–0.17	0.89–0.91	0.97–0.98
32_bin	0.86–0.88	0.88–0.90	0.80–0.82	0.83–0.85	0.44–0.50	0.44–0.49	0.93–0.94	0.97–0.98
64_bin	0.51–0.63	0.80–0.84	0.74–0.76	0.71–0.74	0.08–0.11	0.18–0.23	~1	0.91–0.92
128_bin	0.64–0.72	0.79–0.81	0.75–0.78	0.77–0.79	0.23–0.28	0.28–0.34	0.95–0.96	0.95–0.96
LoG_sigma.0.5	0.80–0.83	0.85–0.88	0.75–0.78	0.78–0.80	0.34–0.39	0.39–0.44	0.91–0.93	0.93–0.94
LoG_sigma.1.0	0.81–0.86	0.89–0.91	0.77–0.79	0.80–0.82	0.24–0.29	0.28–0.33	0.97–0.98	~1
LoG _sigma.1.5	0.75–0.82	0.78–0.82	0.78–0.81	0.77–0.79	0.24–0.28	0.18–0.22	~1	~1
LoG _sigma.2.0	0.67–0.74	0.89–0.91	0.75–0.78	0.80–0.82	0.13–0.18	0.29–0.34	~1	~1
LoG _sigma.2.5	0.81–0.85	0.79–0.84	0.76–0.78	0.78–0.81	0.24–0.28	0.29–0.34	0.95–0.96	0.97–0.98
LoG _sigma.3.0	0.70–0.75	0.63–0.71	0.74–0.76	0.70–0.72	0.18–0.23	0.14–0.18	0.95–0.96	0.91–0.92
LoG _sigma.3.5	0.59–0.68	0.79–0.82	0.74–0.76	0.74–0.76	0.13–0.17	0.08–0.12	0.97–0.98	~1
LoG _sigma.4.0	0.85–0.87	0.84–0.88	0.77–0.80	0.80–0.82	0.29–0.34	0.29–0.34	0.95–0.96	~1
LoG _sigma.4.5	0.63–0.68	0.55–0.62	0.73–0.75	0.74–0.77	0.09–0.12	0.13–0.17	0.97–0.98	0.97–0.98
LoG _sigma.5.0	0.84–0.86	0.74–0.79	0.77–0.79	0.76–0.78	0.23–0.28	0.19–0.23	0.97–0.98	0.97–0.98
Wav_HHH	0.81–0.84	0.81–0.84	0.77–0.79	0.77–0.80	0.23–0.28	0.19–0.24	0.97–0.98	~1
Wav_HHL	0.65–0.71	0.83–0.85	0.75–0.78	0.75–0.78	0.13–0.17	0.13–0.17	~1	~1
Wav_HLH	0.72–0.76	0.53–0.61	0.76–0.78	0.76–0.78	0.18–0.23	0.19–0.23	0.97–0.98	0.97–0.98
Wav_HLL	0.86–0.89	0.91–0.92	0.77–0.79	0.75–0.78	0.29–0.34	0.23–0.28	0.95–0.96	0.95–0.96
Wav_LHH	0.76–0.79	0.81–0.85	0.76–0.79	0.78–0.81	0.33–0.38	0.34–0.39	0.93–0.94	0.95–0.96
Wav_LHL	0.83–0.85	0.82–0.85	0.76–0.78	0.77–0.79	0.29–0.34	0.28–0.33	0.93–0.94	0.95–0.96
Wav_LLH	0.71–0.78	0.88–0.90	0.73–0.75	0.78–0.80	0.03–0.06	0.23–0.28	~1	~1
Wav_LLL	0.69–0.75	0.77–0.82	0.76–0.78	0.76–0.78	0.24–0.29	0.29–0.34	0.95–0.96	0.93–0.94

Table 4
Area under the receiver operating characteristic (ROC) curve (AUROC), Accuracy, Sensitivity and Specificity with 95% CI for radiomics and Radiomics + Clinic for different image feature sets using the GLM model.

GLM	AUROC (95% CI)		Accuracy (95% CI)		Sensitivity (95% CI)		Specificity (95% CI)	
Image	Radiomics	Radiomics + Clinic	Radiomics	Radiomics + Clinic	Radiomics	Radiomics + Clinic	Radiomics	Radiomics + Clinic
Original image	0.77–0.81	0.85–0.88	0.79–0.81	0.81–0.83	0.34–0.39	0.44–0.50	0.95–0.96	0.95–0.96
32_bin	0.84–0.86	0.94–0.95	0.83–0.85	0.84–0.86	0.49–0.54	0.71–0.76	0.95–0.96	0.89–0.91
64_bin	0.78–0.81	0.93–0.94	0.83–0.85	0.92–0.93	0.49–0.55	0.76–0.80	0.95–0.96	0.97–0.98
128_bin	0.75–0.78	0.90–0.92	0.77–0.79	0.86–0.88	0.28–0.33	0.60–0.66	0.95–0.96	0.95–0.96
LoG_sigma.0.5	0.81–0.84	0.90–0.92	0.83–0.85	0.84–0.86	0.50–0.55	0.60–0.65	0.95–0.96	0.93–0.94
LoG_sigma.1.0	0.75–0.78	0.92–0.94	0.80–0.82	0.84–0.86	0.45–0.50	0.61–0.66	0.93–0.94	0.93–0.94
LoG _sigma.1.5	0.78–0.81	0.91–0.93	0.78–0.80	0.81–0.83	0.39–0.44	0.66–0.71	0.93–0.94	0.86–0.89
LoG _sigma.2.0	0.76–0.79	0.88–0.90	0.75–0.78	0.78–0.80	0.33–0.39	0.44–0.50	0.91–0.93	0.91–0.93
LoG _sigma.2.5	0.80–0.82	0.89–0.90	0.76–0.78	0.80–0.82	0.39–0.45	0.50–0.55	0.89–0.91	0.91–0.93
LoG _sigma.3.0	0.74–0.77	0.84–0.86	0.77–0.79	0.80–0.82	0.29–0.34	0.39–0.45	0.95–0.96	0.95–0.96
LoG _sigma.3.5	0.67–0.71	0.78–0.82	0.73–0.75	0.78–0.81	0.08–0.12	0.33–0.39	0.97–0.98	0.95–0.96
LoG _sigma.4.0	0.75–0.79	0.89–0.91	0.80–0.82	0.80–0.82	0.39–0.44	0.49–0.55	0.95–0.96	0.91–0.93
LoG _sigma.4.5	0.73–0.76	0.82–0.84	0.77–0.79	0.78–0.81	0.23–0.28	0.34–0.39	0.97–0.98	0.95–0.96
LoG _sigma.5.0	0.79–0.82	0.84–0.86	0.81–0.83	0.83–0.85	0.44–0.49	0.49–0.55	0.95–0.96	0.95–0.96
Wav_HHH	0.81–0.83	0.86–0.88	0.80–0.82	0.84–0.86	0.45–0.50	0.54–0.60	0.93–0.94	0.95–0.96
Wav_HHL	0.80–0.83	0.89–0.91	0.75–0.78	0.86–0.88	0.33–0.39	0.60–0.65	0.91–0.92	0.95–0.96
Wav_HLH	0.81–0.84	0.89–0.91	0.78–0.80	0.85–0.86	0.38–0.44	0.55–0.61	0.93–0.94	0.95–0.96
Wav_HLL	0.77–0.80	0.88–0.90	0.78–0.80	0.83–0.85	0.38–0.44	0.55–0.60	0.93–0.94	0.93–0.94
Wav_LHH	0.83–0.85	0.91–0.92	0.83–0.85	0.84–0.86	0.49–0.55	0.60–0.65	0.95–0.96	0.93–0.94
Wav_LHL	0.89–0.91	0.93–0.94	0.81–0.83	0.82–0.84	0.55–0.60	0.60–0.66	0.91–0.93	0.89–0.91
Wav_LLH	0.76–0.79	0.90–0.92	0.73–0.75	0.86–0.87	0.29–0.34	0.65–0.71	0.89–0.91	0.93–0.94
Wav_LLL	0.76–0.79	0.85–0.87	0.81–0.83	0.83–0.85	0.33–0.38	0.55–0.61	~1	0.93–0.94

3. Results

The prognostic performance of 4 machine learning algorithms was evaluated for patient outcome prediction. Tables 2–5 show the evaluated performance metrics for models constructed using radiomic features combined with clinical data.

Table 2 provides a detailed analysis of the SVM model using different image processing techniques. For the SVM model, the best results were observed when combining image data filtered by the wavelet and clinical data (AUROC, accuracy, sensitivity, and specificity with 95% confidence interval were 0.88–0.90, 0.85–0.86, 0.50–0.55 and 0.97–0.98, respectively). Table 3 summarizes the results achieved by the KNN models in different image processing methods. For the KNN model, the best results were observed when combining image data resampled to 32 bins and clinical data (AUROC, accuracy, sensitivity, and specificity with 95% confidence interval were 0.88–0.90, 0.83–0.85, 0.44–0.49 and 0.97–0.98, respectively).

Table 4 presents the results achieved by the GLM model when using different image processing methods. For the GLM model, the best results were observed when combining image data resampled to 64 bins and clinical data (AUROC, accuracy, sensitivity, and specificity with 95% confidence interval were 0.93–0.94, 0.92–0.93, 0.76–0.80, and 0.97–0.98, respectively). Table 5 summarizes the results obtained by XGBoost model using different image processing methods. The best performance was achieved by the XGBoost model when combining radiomics analysis and patient's stage and grade (AUROC, accuracy, sensitivity, and specificity with 95% confidence interval were 0.97, 0.98, 0.93–0.96 and ~1, respectively).

Table 5
Area under the receiver operating characteristic (ROC) curve (AUROC), Accuracy, Sensitivity and Specificity with 95% CI for radiomics and Radiomics + Clinic for different image feature sets using the XGBoost model.

Xgboost	AUROC (95% CI)		Accuracy (95% CI)		Sensitivity (95% CI)		Specificity (95% CI)	
Image	Radiomics	Radiomics + Clinic	Radiomics	Radiomics + Clinic	Radiomics	Radiomics + Clinic	Radiomics	Radiomics + Clinic
Original image	0.97–0.99	0.97–0.98	0.95–0.96	0.95–0.96	0.81–0.85	0.81–0.85	~1	~1
32_bin	0.96–0.97	0.96–0.99	0.95–0.97	0.96–0.97	0.78–0.80	0.87–0.91	~1	~1
64_bin	0.97–0.98	0.97–0.98	0.95–0.96	0.92–0.93	0.82–0.86	071–076	~1	~1
128_bin	0.97–0.99	0.96–0.98	0.93–0.95	0.94–0.98	0.77–0.81	0.93–0.95	~1	~1
LoG_sigma.0.5	0.95–0.98	0.97–0.98	0.89–0.91	0.90–0.91	0.60–0.66	0.65–0.70	~1	~1
LoG_sigma.1.0	0.94–0.96	0.87–0.89	0.81–0.83	0.77–0.79	0.33–0.39	0.18–0.23	~1	~1
LoG _sigma.1.5	0.96–0.97	0.96–0.97	0.87–0.89	0.90–0.92	0.59–0.65	0.71–0.76	0.97–0.98	~1
LoG _sigma.2.0	0.95–0.98	0.96–0.97	0.90–0.92	0.95–0.98	0.71–0.76	0.93–0.96	0.97–0.98	~1
LoG _sigma.2.5	0.86–0.89	0.96–0.98	0.86–0.88	0.96–0.98	0.49–0.55	0.93–0.95	~1	~1
LoG _sigma.3.0	0.91–0.93	0.85–0.87	0.83–0.85	0.81–0.83	0.55–0.60	0.44–0.49	0.93–0.95	0.95–0.96
LoG _sigma.3.5	0.91–0.93	0.86–0.88	0.87–0.89	0.81–0.83	0.65–0.70	0.44–0.50	0.95–0.90	0.95–0.96
LoG _sigma.4.0	0.83–0.85	0.83–0.85	0.81–0.84	0.81–0.83	0.34–0.39	0.34–0.39	~1	~1
LoG _sigma.4.5	0.92–0.94	0.97–0.98	0.84–0.86	0.86–0.88	0.44–0.50	0.54–0.60	~1	0.97–0.98
LoG _sigma.5.0	0.97–0.98	0.97–0.99	0.90–0.92	0.93–0.95	0.66–0.71	0.77–0.81	~1	~1
Wav_HHH	0.97–0.99	0.96–0.99	0.93–0.95	0.96–0.97	0.82–0.86	0.93–0.95	0.97–0.98	0.97–0.98
Wav_HHL	0.82–0.85	0.95–0.96	0.81–0.83	0.89–0.90	0.38–0.44	0.65–0.71	0.97–0.98	0.97–0.98
Wav_HLH	0.85–0.87	0.94–0.96	0.81–0.83	0.83–0.85	0.81–0.83	0.39–0.44	0.95–0.96	~1
Wav_HLL	0.86–0.88	0.93–0.95	0.83–0.85	0.89–0.90	0.50–0.55	0.60–0.66	0.95–0.96	~1
Wav_LHH	0.96–0.99	0.97–0.98	0.95–0.96	0.87–0.89	0.81–0.85	0.55–0.60	~1	~1
Wav_LHL	0.94–0.96	0.96–0.99	0.80–0.82	0.96–0.97	0.29–0.34	0.87–0.91	~1	0.96–0.97
Wav_LLH	0.95–0.99	0.97–0.99	0.93–0.94	0.96–0.97	0.88–0.91	0.87–0.91	0.95–0.96	0.96–0.97
Wav_LLL	0.88–0.90	0.93–0.94	0.83–0.85	0.78–0.81	0.45–0.50	0.23–0.28	0.94–0.98	~1

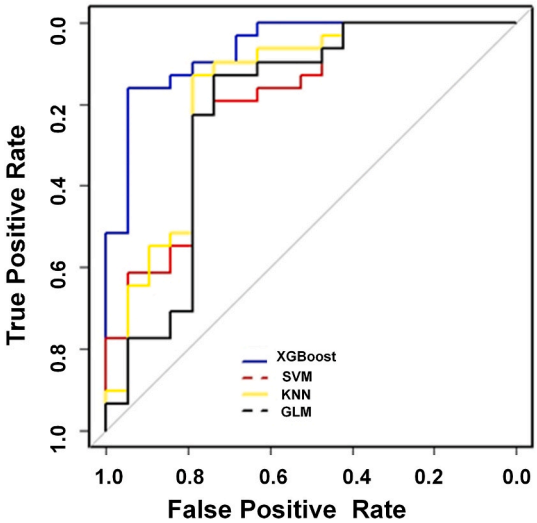

Fig. 2. Area under the ROC curve (AUC) of four different machine learning models (randomly selected from the bootstrap).

Image resampling to a lower number of bins results in better model performance. In addition, combining imaging with clinical data (patient's stage and grade) to create prognostic models achieve better results compared to using only imaging data (the sensitivity was 0.93–0.96 vs 0.71–0.76). The AUROC are depicted in Fig. 2 for different classification models. The top 5 selected features using the MRMR algorithm are visualized on the feature map shown in Fig. 3.

The best single performance among the explored 8 different models was achieved by the XGBoost model through combining radiomic features and patient's stage and grade (AUROC, accuracy, sensitivity, and specificity with 95% confidence interval were 0.97, 0.98, 0.93–0.96 and ~1, respectively).

4. Discussion

Developing a prognostic model is a key tool for individualized therapy of cancer patients. The TNM classification system is the most widely adopted prognostic model for localized RCC patients. However, the TNM staging system is not a a generalizable prognostic model for RCC patients [74], as some factors, such as age, nuclear grading, and tumor necrosis, are ignored [61,62]. The SSIGN score showed higher predictive performance than the TNM staging approach; however, these models are prone to errors because of inter-observer variability as the preponderance of the variability in outcome remains unexplained by these models [62,63].

There is an increasing interest in linking genomics data with patient outcomes for RCC tumors. Zhang et al. [64] assessed the utility of long non-coding RNA to improve prognostic prediction in ccRCC. Their results showed that the 11-lncRNA signature exhibited a better prediction performance for both 3- and 5-year overall survival than the TNM stage (AUROC of approximately 0.80 versus 0.69), which is significantly higher than of the current clinical indicators (TNM and SSIGN score system). Ha et al. [65] determined the role of TMED3 gene in RCC tumors prognosis between low-stage (Stage I and II) and high-stage (Stage III and IV) patients in The Cancer Genome Atlas (TCGA) and The International Cancer Genome Consortium (ICGC) cohorts. The AUROC for low-stage and high-stage was similar 0.56. Recently Hu et al. [66] preformed a study of survival prediction for kidney RCC by combining DNA methylation analysis and gene expression data analysis using the LASSO Cox regression risk score model. In Hu et al. [66], the enrolled patients were divided into high- and low-risk groups, where the reported risk score based on the seven methylated-differentially expressed genes performed well in death prediction survival analysis (AUROC was 0.71 for 5 years). Shi et al. [67] stratified samples into low- and high-risk groups. They showed that survival rate was markedly different between the two groups using the multivariable Cox regression model (AUROC was 0.819). More recently, Zeng et al. [68] developed a prognosis model for ccRCC patients based on a six-lncRNA-based risk score (using RNA sequence data) where he training and validation sets showed similar performance (AUROC at 5 years of 0.649 and 0.681, respectively).

Previously, radiomic models were applied on different cancer types to provide a perspective on risk of death. Shayesteh et al. [69] developed a radiomics-based machine learning model for 2-year survival prediction in lung cancer. They reported a sensitivity of 80% using a logistic regression model. Wang et al. [41] developed a model using MRI radiomics for 5-year survival prediction in hepatocellular carcinoma

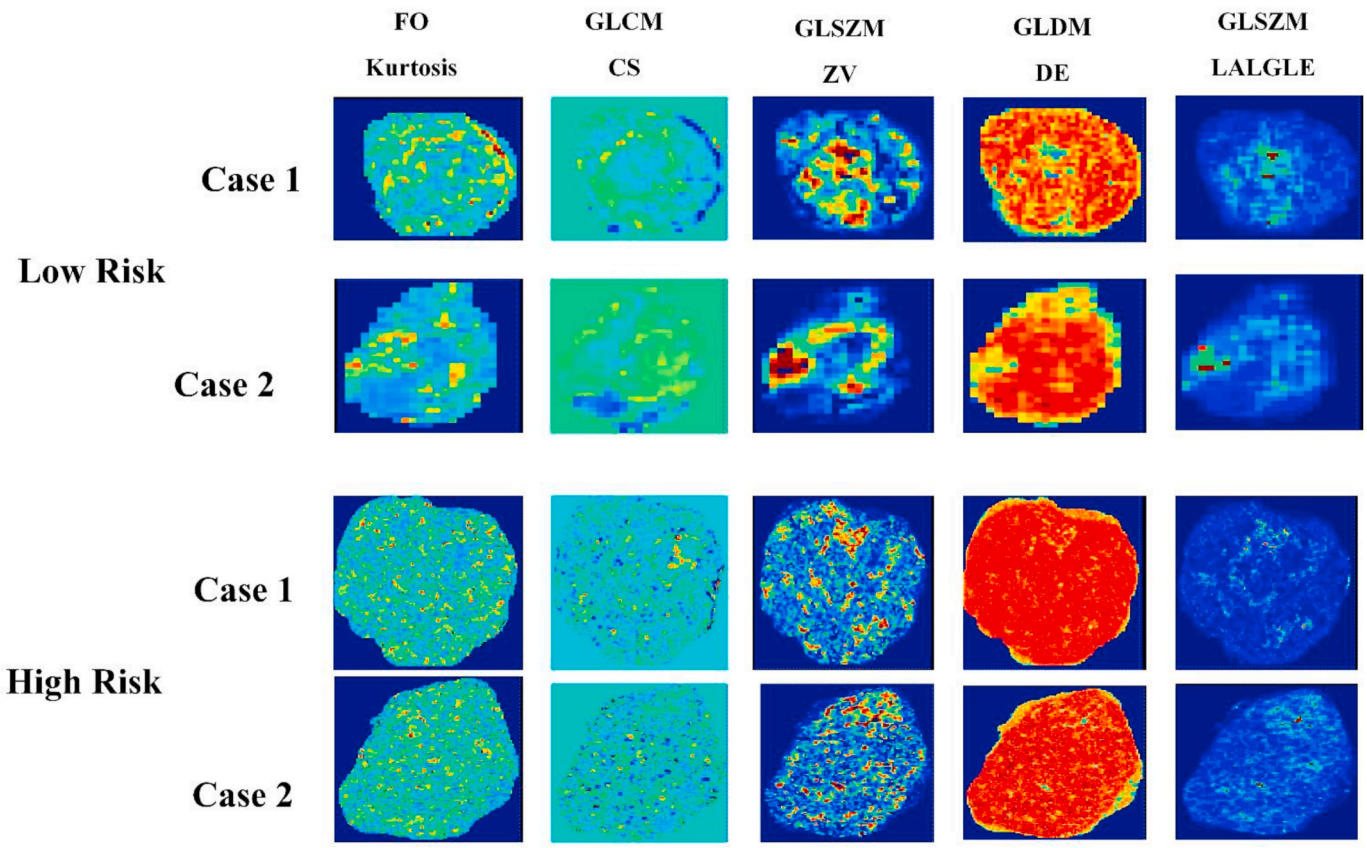

Fig. 3. Feature map of important features in XGBoost model for two high- and low-risk patients.

patients and reported a mean AUC of 0.980 and 0.757 in the training and validation sets, respectively.

For the development of radiomics risk models, a variety of algorithms were designed and are available for end-users [70,71]. However, it is not clear which algorithm provides optimal results [70,72]. In the current study, we used 4 popular classification algorithms to figure out which one provides the best performance on our dataset. The XGBoost model combining radiomic features and patient's stage and grade (AUROC, accuracy, sensitivity, and specificity with 95% confidence interval were 0.95–0.98, 0.97–0.98, 0.93–0.98, 0.93–0.96 and ~1.0, respectively) provided the best performance among all prediction models. In our work, the sensitivity reports how well a model can detect high-risk patients who are actually at high-risk. Therefore, this is a significant parameter for models' evaluation. In this work, among the different models, only the widely used XGBoost (efficient and easy to use algorithm) demonstrated acceptable sensitivity whereas the other models resulted in disappointing sensitivity. As the different methods provided a sensitivity less than 0.5 and high AUC, specificity and accuracy, assessing different evaluation metrics of the radiomics model is necessary to address the dark side of radiomics [73].

The current work inherently bears a number of limitations, including the retrospective nature of the study and the small sample size with no external validation data set. However, we used the bootstrap technique to evaluate our models to address the issue of limited sample size. Future studies will exploit the proposed prognostic model using a large size of external validation set emanating from a multicenter study.

5. Conclusion

In conclusion, we developed a radiomics model providing more accurate prediction of overall survival in RCC patients for estimating prognosis in RCC patients. The XGBoost model combining radiomic features on images filtered by the LoG filter and clinical information provided the highest performance among all prediction models.

Declaration of competing interest

PLEASE CHECK THE FOLLOWING AS APPROPRIATE.

All authors have participated in (a) conception and design, or analysis and interpretation of the data; (b) drafting the article or revising it critically for important intellectual content; and (c) approval of the final version.
The Article I have submitted to the journal for review is original, has been written by the stated authors and has not been published elsewhere.
The Images that I have submitted to the journal for review are original, was taken by the stated authors, and has not been published elsewhere.
This manuscript has not been submitted to, nor is under review at, another journal or other publishing venue.
The authors have no affiliation with any organization with a direct or indirect financial interest in the subject matter discussed in the manuscript

Acknowledgments

This work was supported by the Swiss National Science Foundation, Switzerland under grant SNRF 320030_176052.

References

[1] F. Bray, J. Ferlay, I. Soerjomataram, R.L. Siegel, L.A. Torre, A. Jemal, Global cancer statistics 2018: GLOBOCAN estimates of incidence and mortality worldwide for 36 cancers in 185 countries, Ca - Cancer J. Clin. 68 (2018) 394–424.

[2] W. Street, Cancer facts & figures 2019, Am. Canc. Soc. 76 (2018).

[3] J.C. Cheville, C.M. Lohse, H. Zincke, A.L. Weaver, M.L. Blute, Comparisons of outcome and prognostic features among histologic subtypes of renal cell carcinoma, Am. J. Surg. Pathol. 27 (2003) 612–624.

[4] T. Gudbjartsson, S. Hardarson, V. Petursdottir, A. Thoroddsen, J. Magnusson, G. V. Einarsson, Histological subtyping and nuclear grading of renal cell carcinoma and their implications for survival: a retrospective nation-wide study of 629 patients, Eur. Urol. 48 (2005) 593–600.

[5] A. Abu-Hanna, P.J. Lucas, Prognostic models in medicine, Methods Inf. Med. 40 (2001) 1–5.

[6] M. Nazari, I. Shiri, G. Hajianfar, N. Oveisi, H. Abdollahi, M.R. Deevband, M. Oveisi, H. Zaidi, Non-invasive Fuhrman grading of clear cell renal cell carcinoma using computed tomography radiomics features and machine learning, Radiol. Med. 125 (8) (2020 Aug) 754–762.

[7] B. Delahunt, Histopathologic prognostic indicators for renal cell carcinoma, Semin. Diagn. Pathol. (1998) 68–76.

[8] A.B. Gelb, Renal cell carcinoma: current prognostic factors, Cancer 80 (1997) 981–986.

[9] M.H. Harmer, TNM Classification of Malignant Tumours, The Union, 1978.

[10] S.L. Hermanek P, TNM Classification of Malignant Tumours, fourth ed., Springer, Berlin, Heidelberg, New York, 1987.

[11] P. Guinan, R. Saffrin, D. Stuhldreher, W. Frank, M. Rubenstein, Renal cell carcinoma: comparison of the TNM and Robson stage groupings, J. Surg. Oncol. 59 (1995) 186–189.

[12] K.S. Hafez, A.F. Fergany, A.C. Novick, Nephron sparing surgery for localized renal cell carcinoma: impact of tumor size on patient survival, tumor recurrence and TNM staging, J. Urol. 162 (1999) 1930–1933.

[13] J.J.P. Alessandro Volpe, Prognostic factors in renal cell carcinoma, World J. Urol. 28 (June 2010).

[14] K.-H. Tsui, O. Shvarts, R.B. Smith, R.A. Figlin, J.B. deKERNION, A. Belldegrun, Prognostic indicators for renal cell carcinoma: a multivariate analysis of 643 patients using the revised 1997 TNM staging criteria, J. Urol. 163 (2000) 1090–1095.

[15] X. Chen, X. Sun, Y. Hoshida, Survival analysis tools in genomics research, Hum. Genom. 8 (2014) 21.

[16] F. Büttner, S. Winter, S. Rausch, A. Reustle, S. Kruck, K. Junker, A. Stenzl, A. Agaimy, A. Hartmann, J. Bedke, Survival prediction of clear cell renal cell carcinoma based on gene expression similarity to the proximal tubule of the nephron, Eur. Urol. 68 (2015) 1016–1020.

[17] T. Okegawa, M. Morimoto, S. Nishizawa, S. Kitazawa, K. Honda, H. Araki, T. Tamura, A. Ando, Y. Satomi, K. Nutahara, Intratumor heterogeneity in primary kidney cancer revealed by metabolic profiling of multiple spatially separated samples within tumors, EBioMedicine 19 (2017) 31–38.

[18] R.J. Gillies, P.E. Kinahan, H. Hricak, Radiomics: images are more than pictures, They are data, Radiology 278 (2016) 563–577.

[19] S.S. Yip, H.J. Aerts, Applications and limitations of radiomics, Phys. Med. Biol. 61 (2016) R150–R166.

[20] K.K. Yan, X. Wang, W.W.T. Lam, V. Vardhanabhuti, A.W.M. Lee, H.H. Pang, Radiomics analysis using stability selection supervised component analysis for right-censored survival data, Comput. Biol. Med. 124 (2020) 103959.

[21] M. Vallières, A. Zwanenburg, B. Badic, C.C. Le Rest, D. Visvikis, M. Hatt, Responsible radiomics research for faster clinical translation, J Nucl Med. 59 (2) (2018) 189–193, https://doi.org/10.2967/jnumed.117.200501.

[22] P. Lambin, R.T. Leijenaar, T.M. Deist, J. Peerlings, E.E. De Jong, J. Van Timmeren, S. Sanduleanu, R.T. Larue, A.J. Even, A. Jochems, Radiomics: the bridge between medical imaging and personalized medicine, Nat. Rev. Clin. Oncol. 14 (2017) 749–762.

[23] W. Sun, B. Zheng, W. Qian, Automatic feature learning using multichannel ROI based on deep structured algorithms for computerized lung cancer diagnosis, Comput. Biol. Med. 89 (2017) 530–539.

[24] Y. Kurata, M. Nishio, A. Kido, K. Fujimoto, M. Yakami, H. Isoda, K. Togashi, Automatic segmentation of the uterus on MRI using a convolutional neural network, Comput. Biol. Med. 114 (2019) 103438.

[25] G. M, A. V, M.-M. S, M. H, Concept attribution: explaining CNN decisions to physicians, Comput. Biol. Med. 123 (2020) 103865.

[26] P. Meyer, V. Noblet, C. Mazzara, A. Lallement, Survey on deep learning for radiotherapy, Comput. Biol. Med. 98 (2018) 126–146.

[27] S. Bonte, I. Goethals, R. Van Holen, Machine learning based brain tumour segmentation on limited data using local texture and abnormality, Comput. Biol. Med. 98 (2018) 39–47.

[28] M. Caballo, D.R. Pangallo, R.M. Mann, I. Sechopoulos, Deep learning-based segmentation of breast masses in dedicated breast CT imaging: radiomic feature stability between radiologists and artificial intelligence, Comput. Biol. Med. 118 (2020) 103629.

[29] G.S. Tandel, A. Balestrieri, T. Jujaray, N.N. Khanna, L. Saba, J.S. Suri, Multiclass magnetic resonance imaging brain tumor classification using artificial intelligence paradigm, Comput. Biol. Med. 122 (2020) 103804.

[30] M. Abadi, P. Barham, J. Chen, Z. Chen, A. Davis, J. Dean, M. Devin, S. Ghemawat, G. Irving, M. Isard, Tensorflow: A System for Large-Scale Machine Learning, 12th {USENIX} Symposium on Operating Systems Design and Implementation ({OSDI} 16), 2016, pp. 265–283.

[31] A. Rahmim, P. Huang, N. Shenkov, S. Fotouhi, E. Davoodi-Bojd, L. Lu, Z. Mari, H. Soltanian-Zadeh, V. Sossi, Improved prediction of outcome in Parkinson's disease using radiomics analysis of longitudinal DAT SPECT images, Neuroimage: Clinical 16 (2017) 539–544.

[32] Q. Feng, Y. Chen, Z. Liao, H. Jiang, D. Mao, M. Wang, E. Yu, Z. Ding, Corpus callosum radiomics-based classification model in alzheimer's disease: a case-control study, Front. Neurol. 9 (2018) 618.

[33] Y. Wu, J.-H. Jiang, L. Chen, J.-Y. Lu, J.-J. Ge, F.-T. Liu, J.-T. Yu, W. Lin, C.-T. Zuo, J. Wang, Use of radiomic features and support vector machine to distinguish Parkinson's disease cases from normal controls, Ann. Transl. Med. 7 (2019).

[34] T. Shiiba, Y. Arimura, M. Nagano, T. Takahashi, A. Takaki, Improvement of classification performance of Parkinson's disease using shape features for machine learning on dopamine transporter single photon emission computed tomography, PloS One 15 (2020), e0228289.

[35] S. Ashrafinia, P. Dalaie, R. Yan, P. Ghazi, C. Marcus, M. Taghipour, P. Huang, M. Pomper, T. Schindler, A. Rahmim, Radiomics analysis of clinical myocardial perfusion SPECT to predict coronary artery calcification, J. Nucl. Med. 59 (2018), 512-512.

[36] S. Ashrafinia, P. Dalaie, R. Yan, P. Huang, M. Pomper, T. Schindler, A. Rahmim, Application of texture and radiomics analysis to clinical myocardial perfusion SPECT imaging, J. Nucl. Med. 59 (2018), 94-94.

[37] M. Kolossváry, J. Karády, B. Szilveszter, P. Kitslaar, U. Hoffmann, B. Merkely, P. Maurovich-Horvat, Radiomic features are superior to conventional quantitative computed tomographic metrics to identify coronary plaques with napkin-ring sign, Circ. Cardiovasc. Imag. 10 (2017), e006843.

[38] U. Neisius, H. El-Rewaidy, S. Nakamori, J. Rodriguez, W.J. Manning, R. Nezafat, Radiomic Analysis of Myocardial Native T1 Imaging Discriminates between Hypertensive Heart Disease and Hypertrophic Cardiomyopathy, JACC Cardiovasc Imaging, 2019.

[39] M. Edalat-Javid, I. Shiri, G. Hajianfar, H. Abdollahi, H. Arabi, N. Oveisi, M. Javadian, M. Shamsaei Zafarghandi, H. Malek, A. Bitarafan-Rajabi, M. Oveisi, H. Zaidi, Cardiac SPECT radiomic features repeatability and reproducibility: a multi-scanner phantom study, J. Nucl. Cardiol. (2020), https://doi.org/10.1007/s12350-020-02109-0. In press.

[40] D. Molina, J. Pérez-Beteta, A. Martínez-González, J. Martino, C. Velásquez, E. Arana, V.M. Pérez-García, Influence of gray level and space discretization on brain tumor heterogeneity measures obtained from magnetic resonance images, Comput. Biol. Med. 78 (2016) 49–57.

[41] X.-H. Wang, L.-H. Long, Y. Cui, A.Y. Jia, X.-G. Zhu, H.-Z. Wang, Z. Wang, C.-M. Zhan, Z.-H. Wang, W.-H. Wang, MRI-based radiomics model for preoperative prediction of 5-year survival in patients with hepatocellular carcinoma, Br. J. Canc. 122 (2020) 978–985.

[42] L.F. Machado, P.C.L. Elias, A.C. Moreira, A.C. Dos Santos, L.O. Murta Junior, MRI radiomics for the prediction of recurrence in patients with clinically non-functioning pituitary macroadenomas, Comput. Biol. Med. 124 (2020) 103966.

[43] S. Mostafaei, H. Abdollahi, S. Kazempour Dehkordi, I. Shiri, A. Razzaghdoust, S. H. Zoljalali Moghaddam, A. Saadipoor, F. Koosha, S. Cheraghi, S.R. Mahdavi, CT imaging markers to improve radiation toxicity prediction in prostate cancer radiotherapy by stacking regression algorithm, Radiol. Med. 125 (2020) 87–97.

[44] Y. Zhang, A. Oikonomou, A. Wong, M.A. Haider, F. Khalvati, Radiomics-based prognosis analysis for non-small cell lung cancer, Sci. Rep. 7 (2017) 46349.

[45] O. Jimenez-Del-Toro, Y. Dicente Cid, A. Platon, A.L. Hachulla, F. Lador, P. A. Poletti, H. Müller, A lung graph model for the radiological assessment of chronic thromboembolic pulmonary hypertension in CT, Comput. Biol. Med. 125 (2020) 103962.

[46] M. Saad, T.-S. Choi, Deciphering unclassified tumors of non-small-cell lung cancer through radiomics, Comput. Biol. Med. 91 (2017) 222–230.

[47] R. Paul, M. Schabath, R. Gillies, L. Hall, D. Goldgof, Convolutional Neural Network ensembles for accurate lung nodule malignancy prediction 2 years in the future, Comput. Biol. Med. 122 (2020) 103882.

[48] B. Zhang, J. Tian, D. Dong, D. Gu, Y. Dong, L. Zhang, Z. Lian, J. Liu, X. Luo, S. Pei, X. Mo, W. Huang, F. Ouyang, B. Guo, L. Liang, W. Chen, C. Liang, S. Zhang, Radiomics features of multiparametric MRI as novel prognostic factors in advanced nasopharyngeal carcinoma, Clin. Canc. Res. 23 (2017) 4259–4269.

[49] X. Mo, X. Wu, D. Dong, B. Guo, C. Liang, X. Luo, B. Zhang, L. Zhang, Y. Dong, Z. Lian, J. Liu, S. Pei, W. Huang, F. Ouyang, J. Tian, S. Zhang, Prognostic value of the radiomics-based model in progression-free survival of hypopharyngeal cancer treated with chemoradiation, Eur. Radiol. 30 (2020) 833–843.

[50] J.E. Park, H.S. Kim, Y. Jo, R.-E. Yoo, S.H. Choi, S.J. Nam, J.H. Kim, Radiomics prognostication model in glioblastoma using diffusion- and perfusion-weighted MRI, Sci. Rep. 10 (2020) 4250.

[51] I. Shiri, G. Hajianfar, A. Sohrabi, H. Abdollahi, P.S. S, P. Geramifar, H. Zaidi, M. Oveisi, A. Rahmim, Repeatability of radiomic features in magnetic resonance imaging of glioblastoma: test-retest and image registration analyses, Med. Phys. (2020), https://doi.org/10.1002/mp.14368. In press.

[52] M.A. Haider, A. Vosough, F. Khalvati, A. Kiss, B. Ganeshan, G.A. Bjarnason, CT texture analysis: a potential tool for prediction of survival in patients with metastatic clear cell carcinoma treated with sunitinib, Canc. Imag. 17 (2017) 4.

[53] M.G. Lubner, N. Stabo, E.J. Abel, A.M. del Rio, P.J. Pickhardt, CT textural analysis of large primary renal cell carcinomas: pretreatment tumor heterogeneity correlates with histologic findings and clinical outcomes, AJR Am. J. Roentgenol. 207 (2016) 96–105.

[54] S. Tabibu, P.K. Vinod, C.V. Jawahar, Pan-Renal Cell Carcinoma classification and survival prediction from histopathology images using deep learning, Sci. Rep. 9 (2019) 10509.

[55] O. Akin, P. Elnajjar, M. Heller, R. Jarosz, B. Erickson, S. Kirk, J. Filippini, Radiology Data from the Cancer Genome Atlas Kidney Renal Clear Cell Carcinoma [TCGA-KIRC] Collection, The Cancer Imaging Archive, 2016.
[56] A. Fedorov, R. Beichel, J. Kalpathy-Cramer, J. Finet, J.C. Fillion-Robin, S. Pujol, C. Bauer, D. Jennings, F. Fennessy, M. Sonka, J. Buatti, S. Aylward, J.V. Miller, S. Pieper, R. Kikinis, 3D slicer as an image computing platform for the quantitative imaging network, Magn. Reson. Imaging 30 (2012) 1323–1341.
[57] J.J. Van Griethuysen, A. Fedorov, C. Parmar, A. Hosny, N. Aucoin, V. Narayan, R. G. Beets-Tan, J.-C. Fillion-Robin, S. Pieper, H.J. Aerts, Computational radiomics system to decode the radiographic phenotype, Canc. Res. 77 (2017) e104–e107.
[58] M. Shafiq-ul-Hassan, G.G. Zhang, K. Latifi, G. Ullah, D.C. Hunt, Y. Balagurunathan, M.A. Abdalah, M.B. Schabath, D.G. Goldgof, D. Mackin, Intrinsic dependencies of CT radiomic features on voxel size and number of gray levels, Med. Phys. 44 (2017) 1050–1062.
[59] A. Zwanenburg, S. Leger, M. Vallières, S. Löck, Image Biomarker Standardisation Initiative, 2016 arXiv preprint arXiv:1612.07003.
[60] M. Abudurexiti, D.W. Ye, Causes of death and conditional survival of renal cell carcinoma, Front. Oncol. 9 (2019) 591.
[61] V. Ficarra, A. Galfano, M. Mancini, G. Martignoni, W. Artibani, TNM staging system for renal-cell carcinoma: current status and future perspectives, Lancet Oncol. 8 (2007) 554–558.
[62] H. Moch, W. Artibani, B. Delahunt, V. Ficarra, R. Knuechel, F. Montorsi, J.-J. Patard, C.G. Stief, T. Sulser, P.J. Wild, Reassessing the current UICC/AJCC TNM staging for renal cell carcinoma, Eur. Urol. 56 (2009) 636–643.
[63] N.S. Vasudev, M. Hutchinson, S. Trainor, R. Ferguson, S. Bhattarai, A. Adeyoju, J. Cartledge, M. Kimuli, S. Datta, D. Hanbury, UK Multicenter Prospective Evaluation of the Leibovich Score in Localized Renal Cell Carcinoma: Performance Has Altered over Time, Urology, 2019.
[64] J. Zhang, X. Zhang, C. Piao, J. Bi, Z. Zhang, Z. Li, C. Kong, A long non-coding RNA signature to improve prognostic prediction in clear cell renal cell carcinoma, Biomed. Pharmacother. 118 (2019) 109079.
[65] X. Li, G. Yin, Y. Zhang, D. Dai, J. Liu, P. Chen, L. Zhu, W. Ma, W. Xu, Predictive power of a radiomic signature based on 18F-FDG PET/CT images for EGFR mutational status in NSCLC, Front. Oncol. 9 (2019).
[66] F. Hu, W. Zeng, X. Liu, A gene signature of survival prediction for kidney renal cell carcinoma by multi-omic data analysis, Int. J. Mol. Sci. 20 (2019) 5720.
[67] S. Shi, S. Ye, X. Wu, M. Xu, R. Zhuo, Q. Liao, Y. Xi, A two-DNA methylation signature to improve prognosis prediction of clear cell renal cell carcinoma, Yonsei Med. J. 60 (2019) 1013–1020.
[68] J.-h. Zeng, W. Lu, L. Liang, G. Chen, H.-h. Lan, X.-Y. Liang, X. Zhu, Prognosis of clear cell renal cell carcinoma (ccRCC) based on a six-lncRNA-based risk score: an investigation based on RNA-sequencing data, J. Transl. Med. 17 (2019) 281.
[69] S. Shayesteh, I. Shiri, A. Karami, R. Hashemian, S. Kooranifar, H. Ghaznavi, A. Shakeri-Zadeh, Predicting lung cancer Patients' survival time via logistic regression-based models in a quantitative radiomic framework, J. Biomed. Phys. Eng. 10 (4) (2019) 479–492, https://doi.org/10.31661/JBPE.V0I0.1027.
[70] I. Shiri, H. Maleki, G. Hajianfar, H. Abdollahi, S. Ashrafinia, M. Hatt, H. Zaidi, M. Oveisi, A. Rahmim, Next-generation radiogenomics sequencing for prediction of EGFR and KRAS mutation status in NSCLC patients using multimodal imaging and machine learning algorithms, Mol. Imag. Biol. 22 (2020) 1132–1148.
[71] G. Hajianfar, I. Shiri, H. Maleki, N. Oveisi, A. Haghparast, H. Abdollahi, M. Oveisi, Noninvasive O6 methylguanine-DNA methyltransferase status prediction in glioblastoma multiforme cancer using magnetic resonance imaging radiomics features: univariate and multivariate radiogenomics analysis, World Neurosurg 132 (2019) e140–e161.
[72] S. Rastegar, M. Vaziri, Y. Qasempour, M.R. Akhash, N. Abdalvand, I. Shiri, H. Abdollahi, H. Zaidi, Radiomics for classification of bone mineral loss: a machine learning study, Diagn. Interv. Imag. (2020).
[73] I. Buvat, F. Orlhac, The dark side of radiomics: on the paramount importance of publishing negative results, J. Nucl. Med. 60 (2019) 1543–1544.
[74] W. Jiang, Q. Guo, C. Wang, Y. Zhu, A nomogram based on 9-lncRNAs signature for improving prognostic prediction of clear cell renal cell carcinoma, Cancer Cell Int 19 (208) (2019), https://doi.org/10.1186/s12935-019-0928-5.